Design of Reference Junction Temperature Swing of Power Module for Thermal Management

Jun Zhang, *Member, IEEE*, Xiong Du, *Member, IEEE*, Cheng Qian, Yuyun Ye, *Member, IEEE*, and Junjie Zhou

***Abstract*—Thermal management is a cost-effective means to improve the lifetime of power module, but it also brings negative influence to the converter. To alleviate the negative effect, this article proposes a strategy to design the reference junction temperature swing based on the distribution characteristics of consumed lifetime and the thermal control efficiency. We show that the selected reference temperature swing, including its type and amplitude, allows each application of thermal control to reduce as much consumed lifetime as possible and, at the same time, to guarantee the performance of the converter. Moreover, this approach does not need to obtain the junction temperature swing in real time, which makes the thermal management simple and efficient. The experimental results are presented to verify the merits of the proposed strategy. This article also evaluates the impact of uncertainties due to the semiconductor parameter variations and performs the error analysis of junction temperature estimation.**

***Index Terms*—Lifetime, power module, reference junction temperature swing, thermal management.**

I. Introduction

DUE to the depletion of fossil-fuel reserves, renewable energy systems have been rapidly developed all around the world. Power modules have been widely used in the converter to achieve energy management and processing [1]. The failure of module, however, leads to the downtime of the converter and further induces the failure of renewable energy system trip-off from the power grid. The importance of the requirement regarding the reliability of power module becomes apparent [2]. Furthermore, the industrial report about wind turbine failures in 23 countries, within the period 2003–2017, suggests that the power module is one of the weakest components in the converter [3], with a lifetime far shorter than the desired one. Thus, there is a pressing need to improve the reliability of power module.

Previous studies have shown that the junction temperature swing ΔT_j is one of the common failure causes of power module [4]. Two commonly encountered junction temperature swings, which occurred on loading change in the power converter, are the fundamental frequency junction temperature swing ($\Delta T_{j,\mathrm{FF}}$) and the mission profile junction temperature swing ($\Delta T_{j,\mathrm{MP}}$) [5]. The former is mainly governed by the output frequency of the converter (i.e., fundamental frequency, 50/60 Hz of the grid converter or the frequency of the generator converter), and the latter by the variation of mission profile, such as the fluctuation of wind speed and ambient temperature. Fig. 1(a) shows the difference between $\Delta T_{j,\mathrm{FF}}$ and $\Delta T_{j,\mathrm{MP}}$. It is known that the power module is less reliable with larger ΔT_j [6]. Thus, the size reduction of ΔT_j can improve the lifetime of the power module.

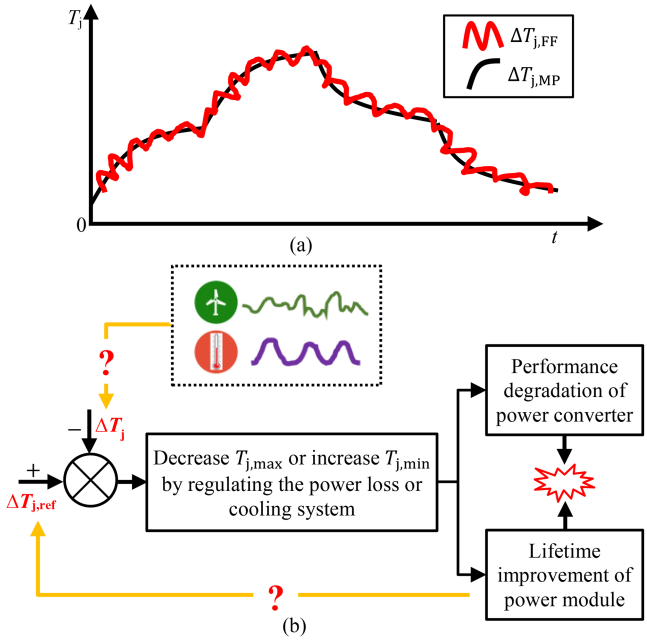

Fig. 1. (a) Schematic curves of $\Delta T_{j,\mathrm{FF}}$ and $\Delta T_{j,\mathrm{MP}}$. (b) Prior-art thermal control techniques.

Manuscript received 1 May 2022; revised 19 July 2022; accepted 19 August 2022. Date of publication 25 August 2022; date of current version 10 October 2022. This work was supported in part by the National Science Foundation of China for Distinguished Young Scholars under Grant 52125704, in part by the National Natural Science Foundation of China under Grant 52107188, in part by the Fundamental Research Funds for Central Universities under Grant B220202007, in part by the Natural Science Foundation of Jiangsu Province under Grant BK20210366, in part by the China Postdoctoral Science Foundation Funded Project under Grant 2020M671316, and in part by the Jiangsu Postdoctoral Research Funding Program under Grant 2020Z315. Recommended for publication by Associate Editor D. G. Lamar. *(Corresponding author: Xiong Du.)*

Jun Zhang is with the College of Energy and Electrical Engineering, Hohai University, Nanjing 211100, China (e-mail: 20190035@hhu.edu.cn).

Xiong Du, Cheng Qian, and Junjie Zhou are with the State Key Laboratory of Power Transmission Equipment and System Security and New Technology, School of Electrical Engineering, Chongqing University, Chongqing 400030, China (e-mail: duxiong@cqu.edu.cn; 20191102018t@cqu.edu.cn; 1837145665@qq.com).

Yuyun Ye is with the Department of Electrical and Computer Engineering, University of Tulsa, Tulsa, OK 74104 USA (e-mail: yuy0104@utulsa.edu).

Color versions of one or more figures in this article are available at https://doi.org/10.1109/TPEL.2022.3201532.

Digital Object Identifier 10.1109/TPEL.2022.3201532

Many thermal management methods have been proposed to reduce the ΔT_j. They can be categorized into two types: the power loss regulation and the cooling condition adjustment. A common practice for the former is to continuously vary the switching frequency [7], [8], [9]. This is mainly due to which the power loss denotes the heat flow in the power module, and the switching loss is proportional to the switching frequency. Similar approaches were also proposed by regulating other loss-related variables, such as the modulation strategy [10], [11], turn-OFF trajectory [12], load current [13], gate resistance [14], reactive current [15], and gate delay time [16]. Besides, it is known that the cooling system affects the heat dissipation in the power module. Thus, ΔT_j can be lowered by adjusting the fan speed of forced air system or the water flow rate of liquid cooling system [17], [18].

Fig. 1(b) illustrates the main idea of the above methods to reduce the ΔT_j. When ΔT_j is higher or lower than $\Delta T_{j,\text{ref}}$, the thermal control is activated to decrease the maximum junction temperature $T_{j,\max}$ or increase the minimum junction temperature $T_{j,\min}$ so as to make the difference of junction temperatures under different loadings small. Then, ΔT_j is lowered and the module lifetime is improved. However, these methods focus on how to reduce the ΔT_j. Few reports have addressed the issue of the selection of reference junction temperature swing $\Delta T_{j,\text{ref}}$. The challenges include two aspects.

1) *How to select the type and amplitude of reference junction temperature swing?:* Accelerated aging tests have shown that the ΔT_j of different periods would affect the reliability of different components in the power module. The short-term ΔT_j (time period in the range of seconds) has significant impact on the bond-wire lift-off, whereas the long-term ΔT_j (time period from minutes to hours) mainly lead to the fatigue of solder layer [4], [19]. $\Delta T_{j,\text{FF}}$ belongs to the short-term ΔT_j and $\Delta T_{j,\text{MP}}$ is the long-term ΔT_j [20]. Since the lifetime of power module depends on the weakest component, the type of $\Delta T_{j,\text{ref}}$ should be taken into account.

Besides, the module lifetime declines as ΔT_j increases [6]. Thus, setting a lower $\Delta T_{j,\text{ref}}$ can reduce more consumed lifetime. However, the thermal control usually has an adverse effect on the performance of the converter. For instance, the technique introduced in [9] reduces the ΔT_j by decreasing the switching frequency. When a smaller $\Delta T_{j,\text{ref}}$ is chosen, smaller switching frequency has to be adopted. This would result in a higher total harmonic distortion (THD), which would worsen the power quality. A higher $\Delta T_{j,\text{ref}}$, on the other hand, reduces the THD but shortens the lifetime. Some methods solve this problem based on the multiobjective optimization. But the multiobjective cost function presents a complex optimization problem and also lacks uniform weighting factors [21]. Thus, it is quite challenging to select the proper $\Delta T_{j,\text{ref}}$.

2) *Difficulty in acquiring the junction temperature swing in real time:* The thermal control should be activated when ΔT_j reaches $\Delta T_{j,\text{ref}}$; otherwise, ΔT_j would exceed $\Delta T_{j,\text{ref}}$ and degrades the performance of thermal control. Thus, the real-time acquisition of ΔT_j is essential. Take the wind energy application as an example. It is easy to obtain the $\Delta T_{j,\text{FF}}$ based on the measured wind speed and pre-established lookup table because $\Delta T_{j,\text{FF}}$ is directly related with a specified wind speed [5]. However, this is not the case for the $\Delta T_{j,\text{MP}}$.

$\Delta T_{j,\text{MP}}$ is related to the wind fluctuations. The maximum and minimum junction temperatures in the $\Delta T_{j,\text{MP}}$ are governed by the wind speeds in different periods [22]. In other words, $\Delta T_{j,\text{MP}}$ depends not only on the current wind speed but also on the future or past wind speed. Due to the unpredictability and the variability of wind speed, wind speed forecasting is still very challenging and time-consuming [23]. Thus, it is not easy to obtain the $\Delta T_{j,\text{MP}}$ in real time. As a result, $\Delta T_{j,\text{ref}}$ has not been well explored.

To address the above two challenges, this article proposes a strategy to design the reference junction temperature swing. The proposed strategy has the following two merits.

1) This method is able to provide a quantitative guidance for the selection of $\Delta T_{j,\text{ref}}$ and to optimize the thermal control while the performance of converter is guaranteed.
2) This method does not need to obtain the $\Delta T_{j,\text{MP}}$ in real time. As a result, the wind speed forecasting can be avoided. This makes the thermal control simple and efficient.

The rest of this article is organized as follows. Section II describes the proposed strategy. Section III shows the impact of this method on the lifetime of power module and the performance of converter. The experimental and case validations are presented in Section IV. Section V analyzes the influence of the error of junction temperature estimation on the result and compares the performance of the proposed method with other techniques. Finally, Section VI concludes this article.

II. Strategy for Reference Junction Temperature Swing

This section presents a strategy to address the challenges on the selection of reference junction temperature swing $\Delta T_{j,\text{ref}}$. Procedure of the proposed strategy is depicted in the flowchart of Fig. 2. The method starts with the estimation of consumed lifetime of power module based on the historical mission profile. Then, the consumed lifetime distributions are analyzed such that the results can be used for determining the type of $\Delta T_{j,\text{ref}}$ as either $\Delta T_{j,\text{FF}}$ or $\Delta T_{j,\text{MP}}$. Next, the thermal control efficiencies under different $\Delta T_{j,\text{ref}}$ are calculated. Finally, proper $\Delta T_{j,\text{ref}}$ is chosen when the thermal control efficiency reaches its maximum value. Details will be given in the following sections.

A. Computation of Junction Temperature Swing

The proposed strategy is based on the module lifetime. Fig. 3 shows the process of consumed lifetime calculation. The detailed analysis can be found in [22]. The wind energy system is chosen for illustration of the proposed strategy. Its parameters are given in Table I. The generator-side converter is considered as a case study and the grid side can share a similar approach for analysis. The power converters adopt two-level back-to-back topology and the bridge arm is made up of two parallel Infineon

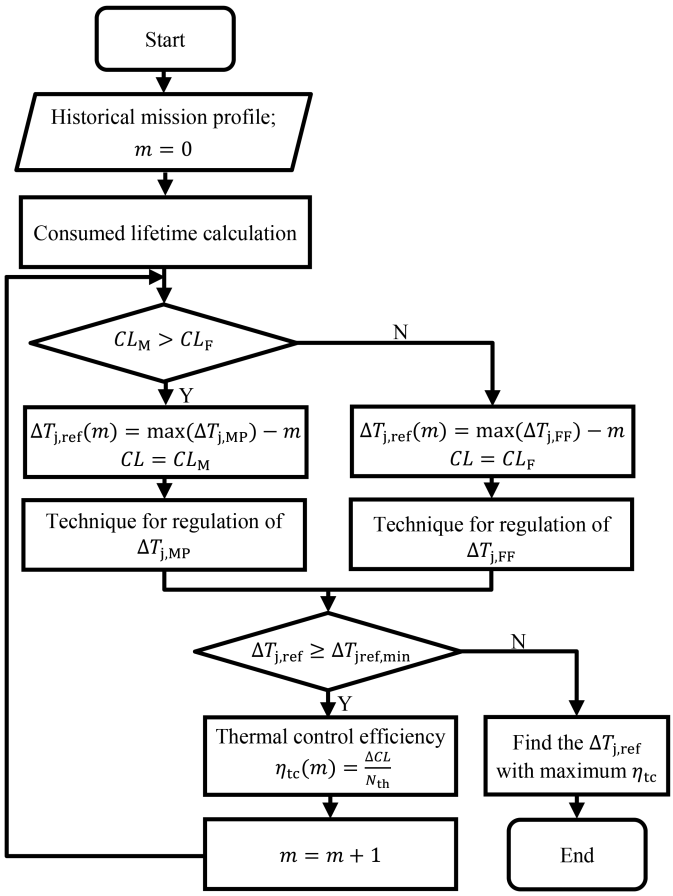

Fig. 2. Procedure of the proposed $\Delta T_{j,\text{ref}}$ design strategy.

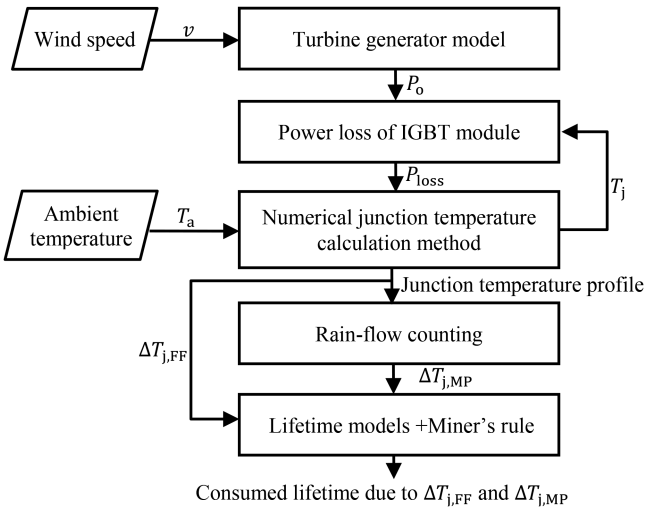

Fig. 3. Flowchart for the consumed lifetime calculation of power module.

FF1000R17IE4 insulated gate bipolar translator (IGBT) modules. One-year mission profiles of the wind speed v and ambient temperature T_a are considered in the computation of consumed lifetime. The data were recorded every minute from Cavan and MalinHead in 2017 [24].

The first step in getting the consumed lifetime is to obtain the output power of converter P_o using the wind speed based on the turbine generator model. Second, the power loss P_{loss} of IGBT module considering the influence of junction temperature T_j is calculated, and the long-term junction temperature profile is generated by the numerical junction temperature calculation method [25]. Fig. 4 shows the calculated junction temperatures in Cavan. The horizontal axis denotes the time sequential mission profile. $T_{j,\max}$ and $T_{j,\min}$ are the maximum and minimum junction temperatures at each mission profile, respectively. Similar results can be obtained in MalinHead.

TABLE I
PARAMETERS OF WIND ENERGY CONVERSION SYSTEM

Parameters	Values
Rated output active power P_r	1.2 MW
Rated voltage for the grid connection point	690 V
Rated switching frequency f_{rated}	3 kHz
DC bus voltage	1100 V
Rated frequency of wind turbine	16 Hz
Cut-in wind speed $v_{\text{cut\_in}}$	2.5 m/s
Rated-wind speed v_{rated}	10.5 m/s
Cut-out wind speed $v_{\text{cut\_out}}$	20 m/s

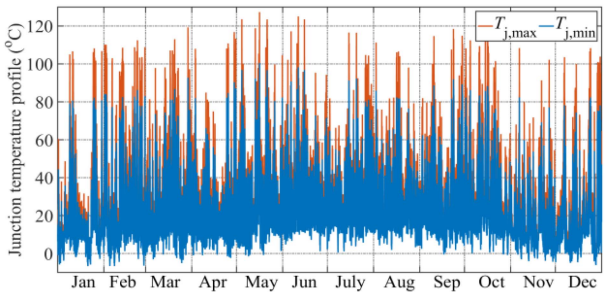

Fig. 4. Junction temperature profile in Cavan.

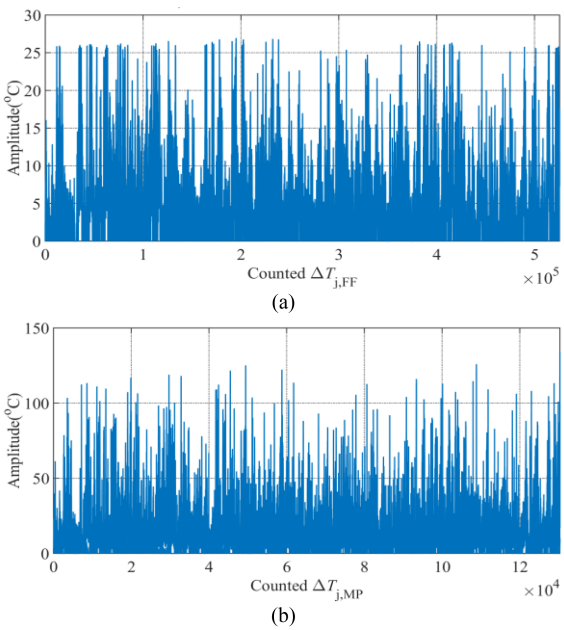

Fig. 5. Counted junction temperature swings in Cavan. (a) $\Delta T_{j,\text{FF}}$. (b) $\Delta T_{j,\text{MP}}$.

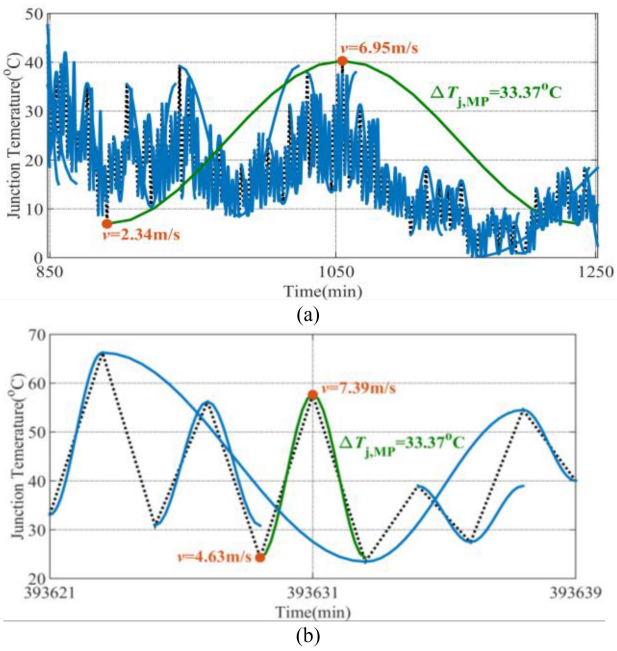

Fig. 6. Same $\Delta T_{j,\mathrm{MP}}$ by different wind speeds at different time intervals. (a) 271th $\Delta T_{j,\mathrm{MP}}$. (b) 98 and 139th $\Delta T_{j,\mathrm{MP}}$. The green curve denotes the intervals at which $\Delta T_{j,\mathrm{MP}} = 33.37\,^{\circ}\mathrm{C}$. The blue curve denotes the intervals at which $\Delta T_{j,\mathrm{MP}}$ is not equal to $33.37\,^{\circ}\mathrm{C}$.

Fig. 5(a) shows the values of counted $\Delta T_{j,\mathrm{FF}}$, and there are 525 600 $\Delta T_{j,\mathrm{FF}}$ in the one-year period. $\Delta T_{j,\mathrm{FF}}$ is obtained by taking the difference between $T_{j,\max}$ and $T_{j,\min}$ at each mission profile in Fig. 4. But this is not so straightforward for $\Delta T_{j,\mathrm{MP}}$ because T_j is randomly fluctuated, as shown in Fig. 4. The rainflow counting method has to be used to convert the randomly changed junction temperature profile into the $\Delta T_{j,\mathrm{MP}}$. Then, $\Delta T_{j,\mathrm{MP}}$ can be obtained by taking the difference between the peak and the valley in the counted cycle. Fig. 5(b) shows the counting results obtained by the rainflow algorithm. There are 130 332 identified $\Delta T_{j,\mathrm{MP}}$.

The procedure to find $\Delta T_{j,\mathrm{MP}}$ is described as follows. Since only the extreme points (valleys and peaks) are needed for the rainflow algorithm, the pole extraction is employed to discard other junction temperatures [26]. For example, if the mean junction temperature is the maximum pole, $T_{j,\max}$ is chosen under this operating condition. After selecting either the maximum or the minimum junction temperature at each wind speed, the temperature profile used for extracting the paths of rainflow is obtained. The junction temperature represents a series of roofs on which the water falls. Each peak and valley are regarded to be the source of the water, which drops down the pagoda. When the drop meets a peak or valley larger than that of departure, the water stops dropping down and the pathway of the waterfall is counted as a half-cycle. When the half-cycle generated by the peak matches the half-cycle generated by the valley, a full-cycle is formed [26].

The junction temperature swing based on mission profile $\Delta T_{j,\mathrm{MP}}$ depends on not only the present wind speed but also on the future or past wind speed. Fig. 6 illustrates the formation of $\Delta T_{j,\mathrm{MP}} = 33.37\,^{\circ}\mathrm{C}$ at different wind speeds at two different cycles. One counted $\Delta T_{j,\mathrm{MP}}$ is determined by T_j at $v = 2.34\,\mathrm{m/s}$ and $v = 6.95\,\mathrm{m/s}$. Another counted $\Delta T_{j,\mathrm{MP}}$ occurs at the T_j of $v = 4.63\,\mathrm{m/s}$ and $v = 7.39\,\mathrm{m/s}$. This phenomenon shows that the wind speeds related to $\Delta T_{j,\mathrm{MP}}$ are not unique. This is different from the $\Delta T_{j,\mathrm{FF}}$, which only depends on the junction temperatures at the present wind speed.

Thermal control is usually activated when the ΔT_j reaches the limit. If the operators want to reduce the $\Delta T_{j,\mathrm{MP}}$ to $30\,^{\circ}\mathrm{C}$ or less, the real-time acquisition of $\Delta T_{j,\mathrm{MP}}$ is necessary for the existing methods. Since $\Delta T_{j,\mathrm{MP}}$ depends on the wind speeds at different cycles, the essence of $\Delta T_{j,\mathrm{MP}}$ acquisition is to forecast the wind speed. However, due to the stochastic characteristic of wind speed, wind speed forecasting is very time-consuming and often makes the thermal control inefficient. It is desirable to develop a method that can reduce the $\Delta T_{j,\mathrm{MP}}$ without acquiring $\Delta T_{j,\mathrm{MP}}$ in real time.

B. Computation of Consumed Lifetime

Two empirical lifetime models are considered to evaluate the consumed lifetime. One is due to the fundamental frequency junction temperature swing $\Delta T_{j,\mathrm{FF}}$, another is due to the mission profile junction temperature swing $\Delta T_{j,\mathrm{MP}}$.

The widely used Bayerer lifetime model from Infineon considers the factors influencing the number of cycles to failure [27], such as the power-ON time t_{on}, the current per wire I, the blocking voltage V, and the diameter of bonding wire D. The number of cycles to failure due to $\Delta T_{j,\mathrm{FF}}$ can be expressed as

$$N_{f,\mathrm{FF}} = k(\Delta T_{j,\mathrm{FF}})^{\beta_1} \cdot e^{\frac{\beta_2}{T_{j,\min}+273}} \cdot t_{\mathrm{on}}^{\beta_3} \cdot I^{\beta_4} \cdot V^{\beta_5} \cdot D^{\beta_6}. \quad (1)$$

The parameter values in (1) are $k = 9.3 \times 10^{14}$, $V = 17$, $D = 300$, $\beta_1 = -4.416$, $\beta_2 = 1285$, $\beta_3 = -0.463$, $\beta_4 = -0.716$, $\beta_5 = -0.761$, and $\beta_6 = -0.5$. This model is tested with the heating time below 15 s. It has been pointed out in [28] that the bond-wire fatigue is highly contributed by the thermal cycles with heating time below 60 s. Since the heating time of fundamental frequency junction temperature swing t_{FF} is smaller than 15 s, the Bayerer model is employed to calculate the $N_{f,\mathrm{FF}}$, which mainly reflects the reliability of bond wire.

Longer thermal cycles (heating time above 60 s) contribute to the solder layer degradation, not the bond-wire degradation [28]. Since heating time of the mission profile junction temperature swing $\Delta T_{j,\mathrm{MP}}$ is usually larger than 60 s, the consumed lifetime due to $\Delta T_{j,\mathrm{MP}}$ primarily considers the reliability of solder layer. On the other hand, the manufacturer of power module provides the accelerated aging test with heating time above 60 s but only gives the relationship between the number of cycles to failure and ΔT_j. Because ΔT_j is more related to the lifetime of power module than the other factors [13] and the proposed strategy focuses on the selection of $\Delta T_{j,\mathrm{ref}}$, the Coffin–Manson model [29] is adopted in the computation of the number of cycles to failure due to mission profile junction temperature swing, which can be expressed as

$$N_{f,\mathrm{MP}} = A \cdot (\Delta T_{j,\mathrm{MP}})^{-\alpha} \quad (2)$$

where $A = 2.25 \times 10^{11}$ and $\alpha = 3.83$.

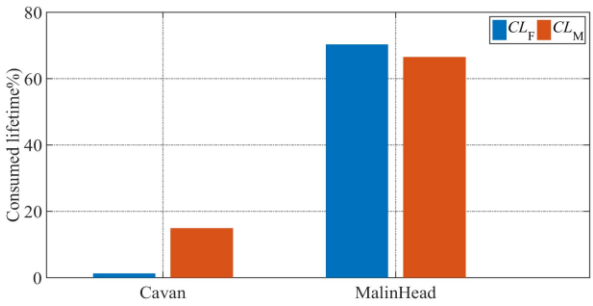

Fig. 7. Consumed lifetimes of power module in Cavan and MalinHead.

The consumed lifetime under junction temperature swing accrues according to Miner's rule and can be expressed as

$$\begin{cases} \mathrm{CL}_F = \sum_{j=1}^{N_{\mathrm{FF}}} \frac{N_{\mathrm{FF},j}}{N_{f\mathrm{FF},j}} \\ \mathrm{CL}_M = \sum_{j=1}^{N_{\mathrm{MP}}} \frac{N_{\mathrm{MP},j}}{N_{f\mathrm{MP},j}} \end{cases} \tag{3}$$

where $N_{f\mathrm{FF},j}$ is the number of cycles to failure caused by the jth $\Delta T_{j,\mathrm{FF}}$ and $N_{\mathrm{FF},j}$ is the number of the jth $\Delta T_{j,\mathrm{FF}}$. N_{FF} denotes the total number of the counted $\Delta T_{j,\mathrm{FF}}$, which is equal to 525 600. $N_{f\mathrm{MP},j}$, $N_{\mathrm{MP},j}$, and N_{MP} have the same meaning corresponding to the mission profile junction temperature swing. Since the reliability of power module depends on the weakest component, and the CL_F and CL_M reflect the lifetimes of bond wire and solder layer, respectively, the consumed lifetime of power module CL is determined as

$$\mathrm{CL} = \max\left(\mathrm{CL}_F, \mathrm{CL}_M\right). \tag{4}$$

When CL is equal to 100%, the power module is rated as failure.

C. Distribution Characteristics of Consumed Lifetime

Fig. 7 shows the consumed lifetimes of power module at different locations. It can be seen from Fig. 7 that CL_M is higher than CL_F in Cavan, which means that the solder layer is likely to fail than the bond wire. According to (4), $\Delta T_{j,\mathrm{MP}}$ is selected as the $\Delta T_{j,\mathrm{ref}}$ in Cavan. This is not the case in MalinHead, where more attention should be paid to the $\Delta T_{j,\mathrm{FF}}$ because $\mathrm{CL}_F > \mathrm{CL}_M$. Thus, the type of $\Delta T_{j,\mathrm{ref}}$ is not fixed. In general, we choose the temperature swing that leads to more consumed lifetime for regulating $\Delta T_{j,\mathrm{ref}}$. For example, if CL_M is larger than CL_F, then $\Delta T_{j,\mathrm{MP}}$ is taken into account. If CL_M is smaller than CL_F, $\Delta T_{j,\mathrm{FF}}$ is considered. This selection scheme can be summarized as

$$\Delta\, T_{j,\mathrm{ref}} = \begin{cases} \Delta T_{j,\mathrm{MP}}, & \text{if } \mathrm{CL}_F < \mathrm{CL}_M \\ \Delta T_{j,\mathrm{FF}}, & \text{if } \mathrm{CL}_F > \mathrm{CL}_M \\ \Delta T_{j,\mathrm{FF}} \text{ or} \Delta T_{j,\mathrm{MP}}, & \text{if } \mathrm{CL}_F = \mathrm{CL}_M. \end{cases} \tag{5}$$

In addition, the distribution of ΔT_j can be defined by the cumulative distribution function

$$p\ \left(\Delta T_j > \Delta T_{j,\mathrm{ref}}\right) = \int_{\Delta T_{j,\mathrm{ref}}}^{\Delta T_{j,\max}} f\left(\Delta T_j\right) d\left(\Delta T_j\right) \tag{6}$$

TABLE II
RELATIONSHIP BETWEEN CL_F AND $\Delta T_{j,\mathrm{FF}}$ IN CAVAN

$\Delta T_{\mathrm{j,ref}}$(°C)	$p(\Delta T_{\mathrm{j,FF}} > \Delta T_{\mathrm{j,ref}})$(%)	$p_{CL_F}(\Delta T_{\mathrm{j,FF}} > \Delta T_{\mathrm{j,ref}})$ (%)
5	31.82	99.94
10	8.02	97.23
15	1.83	84.63
20	0.51	63.77
25	0.19	38.73

TABLE III
RELATIONSHIP BETWEEN CL_M AND $\Delta T_{j,\mathrm{MP}}$ IN CAVAN

$\Delta T_{\mathrm{j,ref}}$(°C)	$p(\Delta T_{\mathrm{j,MP}} > \Delta T_{\mathrm{j,ref}})$(%)	$p_{CL_M}(\Delta T_{\mathrm{j,MP}} > \Delta T_{\mathrm{j,ref}})$ (%)
40	3.08	78.22
60	0.85	53.32
80	0.19	25.73
100	0.04	10.79
120	<0.01	1.64

where $\Delta T_{j,\max}$ is the maximum junction temperature swing. The frequency of junction temperature swing $f(\Delta T_j)$ is defined by

$$f\left(\Delta T_j\right) = \frac{n\left(\Delta T_j\right)}{N} \tag{7}$$

where $n(\Delta T_j)$ denotes the number of ΔT_j and N is the total number of junction temperature swings. Then, the distribution of the consumed lifetime can be obtained by

$$p_{\mathrm{CL}}\ \left(\Delta T_j > \Delta T_{j,\mathrm{ref}}\right) = \frac{\int_{\Delta T_{j,\mathrm{ref}}}^{\Delta T_{j,\max}} \mathrm{CL}\left(\Delta T_j\right) d\left(\Delta T_j\right)}{\mathrm{CL}} \tag{8}$$

where $\mathrm{CL}(\Delta T_j)$ is the consumed lifetime due to the ΔT_j and the CL is the consumed lifetime due to all junction temperature swings.

Table II presents the distribution characteristics of junction temperature swing and consumed lifetime in Cavan from the perspective of fundamental frequency and Table III from the mission profile. It can be seen from Tables II and III that most consumed lifetimes are caused by large junction temperature swings, although there are not many large swings. For example, when $\Delta T_{j,\mathrm{ref}}$ is 20 °C, $p(\Delta T_{j,\mathrm{FF}} > \Delta T_{j,\mathrm{ref}})$ is 0.51%, but $p_{\mathrm{CL}_F}(\Delta T_{j,\mathrm{FF}} > \Delta T_{j,\mathrm{ref}})$ is 63.77%. This implies that $\Delta T_{j,\mathrm{FF}} > 20\,^{\circ}\mathrm{C}$ only accounts for 0.51% of the total $\Delta T_{j,\mathrm{FF}}$, but it accounts for 63.77% of the total consumed lifetimes due to $\Delta T_{j,\mathrm{FF}}$. In other words, the percentage of $\Delta T_{j,\mathrm{FF}} \leq 20\,^{\circ}\mathrm{C}$ is 99.49%, but only 36.23% of the CL_F is caused by $\Delta T_{j,\mathrm{FF}} \leq 20\,^{\circ}\mathrm{C}$. Large junction temperature swings contribute to most consumed lifetimes. Thus, smoothing the large ΔT_j would be more cost-effective. In addition, the value of $\Delta T_{j,\mathrm{FF}}$ is much smaller than that of $\Delta T_{j,\mathrm{MP}}$, as can be seen from Tables II and III. Thus, $\Delta T_{j,\mathrm{FF}}$ and $\Delta T_{j,\mathrm{MP}}$ should be taken care of separately. Similar results can be found in MalinHead.

D. Thermal Control Efficiency

Smaller $\Delta T_{j,\mathrm{ref}}$ can reduce more consumed lifetime of power module but the thermal control has more adverse impact on the converter performance. Take the thermal control based on the switching frequency modulation as an example. Fig. 8 displays

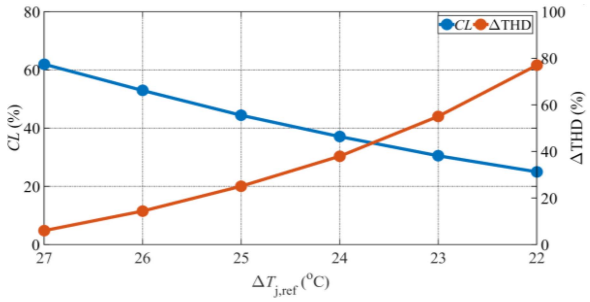

Fig. 8. Impacts of different $\Delta T_{j,\text{ref}}$ on the CL and THD.

the consumed lifetime and the change of THD (ΔTHD) for various $\Delta T_{j,\text{ref}}$. It can be seen from Fig. 8 that CL decreases while the THD rises as $\Delta T_{j,\text{ref}}$ decreases. Thus, thermal control improves the reliability of power module, but at the same time, the power quality declines. It is not straightforward to select the proper $\Delta T_{j,\text{ref}}$.

$\Delta T_{j,\text{ref}}$ also has a drastic impact on THD. It is observed from Fig. 8 that $\Delta\text{THD} = 77\%$ at $\Delta T_{j,\text{ref}} = 22\,^{\circ}\text{C}$, while $\Delta\text{THD} = 55\%$ at $\Delta T_{j,\text{ref}} = 23\,^{\circ}\text{C}$. Moreover, it can be seen from Fig. 8 that larger $\Delta T_{j,\text{ref}}$ causes smaller change in THD, while smaller $\Delta T_{j,\text{ref}}$ causes larger change in THD. In addition, $\Delta T_{j,\text{ref}}$ has a direct influence on the reliability of device. For example, $\text{CL} = 62\%$ under $\Delta T_{j,\text{ref}} = 27\,^{\circ}\text{C}$ and $\text{CL} = 52\%$ under $\Delta T_{j,\text{ref}} = 26\,^{\circ}\text{C}$. Difference of 1° in $\Delta T_{j,\text{ref}}$ can lead to about 10% difference in the consumed lifetime. Therefore, it should be watched carefully even for a few degrees difference in $\Delta T_{j,\text{ref}}$.

The thermal control efficiency η_{tc} is proposed to alleviate the negative impact. It is defined as

$$\eta_{\text{tc}} = \frac{\Delta\text{CL}}{N_{\text{th}}}. \tag{9}$$

ΔCL denotes the reduced consumed lifetime after thermal control. The key of η_{tc} lies in how to obtain the N_{th}, which represents the number of thermal control under $\Delta T_{j,\text{ref}}$. Since ΔT_j is not always larger than $\Delta T_{j,\text{ref}}$ during the operation period, N_{th} is countable. The thermal control should be employed to avoid the situation that the junction temperature swing ΔT_j exceeds $\Delta T_{j,\text{ref}}$ when ΔT_j is close to $\Delta T_{j,\text{ref}}$. Thus, N_{th} depends on $\Delta T_{j,\text{ref}}$. Since ΔT_j is closely related to the wind speed, N_{th} can be obtained by counting the number of wind speeds, which are higher than the threshold wind speed in the one-year period. That is

$$N_{\text{th}} = n\left(v \geq v_{\text{th}}\right). \tag{10}$$

The threshold wind speed v_{th} is the wind speed above which $\Delta T_j \geq \Delta T_{j,\text{ref}}$ would be induced and the thermal control would be applied. Note that v_{th} depends on $\Delta T_{j,\text{ref}}$. If $\Delta T_{j,\text{ref}}$ is $\Delta T_{j,\text{FF}}$, then v_{th} can be obtained by

$$\begin{cases} \Delta T_{j\text{FF,max}}\left(v \geq v_{\text{th}}\right) \geq \Delta T_{j,\text{ref}} \\ \Delta T_{j\text{FF,max}}\left(v < v_{\text{th}}\right) < \Delta T_{j,\text{ref}}. \end{cases} \tag{11}$$

In (11), $\Delta T_{j\text{FF,max}}(v \geq v_{\text{th}}) \geq \Delta T_{j,\text{ref}}$ means that when the wind speed is higher than a threshold v_{th}, the maximum fundamental frequency junction temperature swing will be larger than the reference junction temperature swing.

This is not the case if $\Delta T_{j,\text{ref}}$ is $\Delta T_{j,\text{MP}}$. The main reason is that the $\Delta T_{j,\text{MP}}$ depends on the junction temperatures at two different wind speeds in two different time intervals. Even the amplitudes of counted $\Delta T_{j,\text{MP}}$ are the same, the determined junction temperatures and wind speeds are totally different, as shown in Fig. 6.

To tackle the situation that it is difficult to find N_{th} from v_{th} when $\Delta T_{j,\text{ref}}$ is $\Delta T_{j,\text{MP}}$, a scheme is developed. The scheme considers an extreme condition, which sets the junction temperature at the valley as the minimum ambient temperature $T_{a,\text{min}}$. It is known [12], [17] that the temperature fluctuation can be reduced by lowering the peak value or increasing the valley value of the junction temperature. Moreover, the junction temperature is equal to the ambient temperature when the converter stops working. If the valley of $\Delta T_{j,\text{ref}}$ is set as $T_{a,\text{min}}$, then the peak of $\Delta T_{j,\text{ref}}$ can be used as the upper limit of junction temperature $T_{j\text{max,ref}}$, which is equal to the sum of $\Delta T_{j,\text{ref}}$ and $T_{a,\text{min}}$. This way, $\Delta T_{j,\text{ref}}$ is considered as fixed. On the other hand, we can control the $\Delta T_{j,\text{MP}}$ not exceeding $\Delta T_{j,\text{ref}}$ by regulating $T_{j,\text{max}}$ to be smaller than $T_{j\text{max,ref}}$. Since the junction temperature increases with the rise of wind speed [22], v_{th} can be found by comparing $T_{j,\text{max}}$ at each wind speed with $T_{j\text{max,ref}}$. Thus, the N_{th} is the number of wind speeds higher than v_{th}. The calculations of N_{th} under $\Delta T_{j,\text{MP}}$ are summarized as

$$\begin{cases} T_{j\text{max,ref}} = T_{a,\text{min}} + \Delta T_{j,\text{ref}} \\ T_{j,\text{max}}\left(v \geq v_{\text{th}}\right) \geq T_{j\text{max,ref}} \\ T_{j,\text{max}}\left(v < v_{\text{th}}\right) < T_{j\text{max,ref}}. \end{cases} \tag{12}$$

In (12), $T_{j,\text{max}}(v \geq v_{\text{th}}) \geq T_{j\text{max,ref}}$ is a situation that when the wind speed is higher than a threshold v_{th}, the maximum junction temperature will be larger than the maximum reference junction temperature. Under this circumstance, it is very likely that $\Delta T_{j\text{FF,max}} \geq \Delta T_{j,\text{ref}}$.

The maximum reference swing $\Delta T_{j\text{ref,max}}$ is equal to the maximum counted junction temperature swing. $\Delta T_{j\text{ref,max}}$ in Cavan and MalinHead are $134\,^{\circ}\text{C}$ and $27\,^{\circ}\text{C}$, respectively. The minimum reference swing $\Delta T_{j\text{ref,min}}$ depends on the temperature control method. This article chooses the switching frequency modulation to illustrate how to determine $\Delta T_{j\text{ref,min}}$. Previous studies have shown that $T_{j,\text{max}}$ and $\Delta T_{j,\text{FF}}$ increase along with the wind speed up to the rated wind speed v_{rated}. On the other hand, $T_{j,\text{max}}$ and $\Delta T_{j,\text{FF}}$ decrease if the switching frequency f_s is lowered. Based on (11) and (12), $\Delta T_{j\text{ref,min}}$ can be obtained by

$$\begin{cases} \Delta T_{j\text{ref,min}}\ \left(\Delta T_{j,\text{FF}}\right) = \Delta T_{j,\text{max}}\ \left(v_{\text{rated}}, f_{\text{min}}\right) \\ \Delta T_{j\text{ref,min}}\ \left(\Delta T_{j,\text{MP}}\right) = T_{j,\text{max}}\left(v_{\text{rated}}, f_{\text{min}}\right) - T_{a,\text{min}}. \end{cases} \tag{13}$$

f_{min} denotes the lower limit of the switching frequency. For instance, this study sets f_{min} to $0.5 f_{\text{rated}}$. It can be adjusted according to the actual requirement. The $\Delta T_{j\text{ref,min}}$ in Cavan and MalinHead are found to be $125\,^{\circ}\text{C}$ and $22\,^{\circ}\text{C}$, respectively.

It should be noted that the primary objective of this article is to find the $\Delta T_{j,\text{ref}}$, not to study the temperature control methods,

TABLE IV
THERMAL CONTROL EFFICIENCIES UNDER DIFFERENT REFERENCE SWINGS

Cavan		MalinHead	
$\Delta T_{\text{j,ref}} = \Delta T_{\text{j,MP}}$ (°C)	η_{tc} (%)	$\Delta T_{\text{j,ref}} = \Delta T_{\text{j,FF}}$ (°C)	η_{tc} (%)
134	2.029	27	0.068
133	2.006		
132	2.054	26	0.133
131	2.007		
130	2.048	25	0.186
129	1.985		
128	2.020	24	0.225
127	1.933		
126	1.961	23	0.255
125	1.889	22	0.274

which have been investigated by many previous pieces of literature. If the switching frequency modulation is not allowed, we can choose other techniques, such as the regulation of cooling fan speed. The cooling fan works when the wind speed is higher than v_{th}. It stops working when the wind speed is below v_{th}. Then, $\Delta T_{j\text{ref,min}}$ can be obtained by replacing f_{min} in (13) with the maximum fan speed $v_{\text{fan,max}}$.

III. RESULTS OF THE PROPOSED STRATEGY

This section shows the result of thermal control efficiencies η_{tc} under different reference swings. It also investigates the impact of the proposed strategy on the consumed lifetime of power module and the performance of power converter. Moreover, the sensitivity of η_{tc} is analyzed by the Monte Carlo simulation.

A. Computed Result of Thermal Control Efficiency

Table IV presents the η_{tc} under different $\Delta T_{j,\text{ref}}$ at two different locations. It can be seen from Table IV that the maximum η_{tc} of 2.054 occurs at $\Delta T_{j,\text{ref}} = 132\,^{\circ}\text{C}$ in Cavan. This result means that the thousand applications of the thermal control can reduce the consumed lifetime of power module by 2.054%. Note that the value of N_{th} is counted in the thousands. On the other hand, at MalinHead, the maximum $\eta_{\text{tc}} = 0.274$ occurs at $\Delta T_{j,\text{ref}} = 22\,^{\circ}\text{C}$. This efficiency quadruples the benefit of thermal control at $\Delta T_{j,\text{ref}} = 27\,^{\circ}\text{C}$ at which $\eta_{\text{tc}} = 0.068$. From the aspect of cost, the maximum η_{tc} optimizes the thermal control in which each application of the thermal control can reduce as much more consumed lifetime as possible. Therefore, η_{tc} not only improves the economic interest of thermal control but also provides a quantitative criterion for operators to select the amplitude of $\Delta T_{j,\text{ref}}$.

B. Effect on Consumed Lifetime of Power Module

Table V presents the effect of the proposed strategy on the reliability of power module. Take the result in Cavan as example. It can be seen from Table V that CL_M is lowered from 14.87% to 10.15%. Furthermore, there is a reduction in CL_F at the same time, although the type of $\Delta T_{j,\text{ref}}$ in Cavan belongs to $\Delta T_{j,\text{MP}}$. This is mainly due to which the $\Delta T_{j,\text{MP}}$ is regulated by lowering the $T_{j,\text{max}}$, while $\Delta T_{j,\text{FF}}$ is the difference between $T_{j,\text{max}}$ and $T_{j,\text{min}}$ at each wind speed. Similar results can be found in MalinHead. These results indicate that the proposed thermal control strategy improves the module lifetime and may lower the cost because the replacement of power module can be reduced.

TABLE V
CONSUMED LIFETIMES WITH AND WITHOUT THERMAL CONTROL

Location	Perform control strategy	CL_{F}(%)	CL_{M}(%)
Cavan	No	1.23	14.87
	Yes	0.79	10.15
MalinHead	No	70.32	66.49
	Yes	24.98	23.57

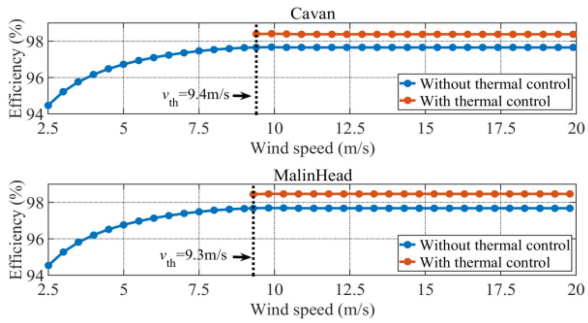

Fig. 9. Impacts of the proposed strategy on the efficiency of power converter.

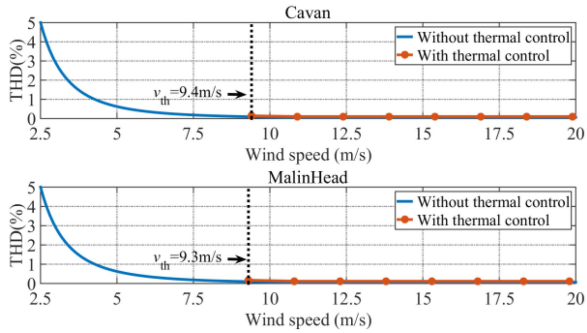

Fig. 10. Impacts of the proposed strategy on the THD.

C. Impact on THD and Converter Efficiency

The impacts of the proposed strategy on THD and converter efficiency are analyzed. Fig. 9 displays the efficiency of the converter versus wind speed with and without the proposed strategy at two different locations, while Fig. 10 displays the THD. It is observed from Fig. 9 that the efficiency is improved after $v \geq v_{\text{th}}$. This is mainly due to which the power loss is reduced when adopting lower switching frequency [7], [9]. In addition, Fig. 10 shows that although the THD rises when the switching frequency is lowered, THD still meets the requirement that THD $\leq 5\%$. Thus, the performance of the power converter can be guaranteed.

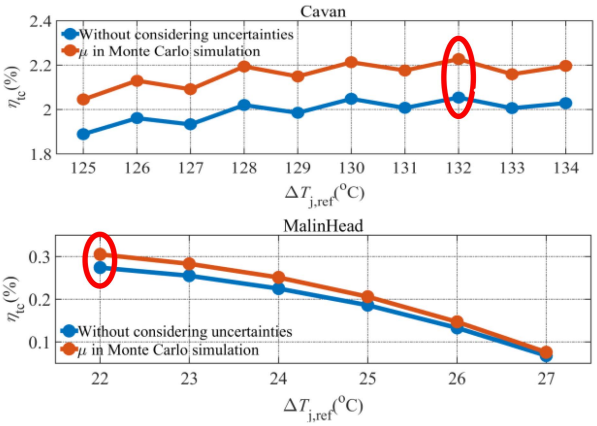

Fig. 11. Monte Carlo analysis of η_{tc}.

D. Monte Carlo Analysis

Monte Carlo simulation is applied to analyze the sensitivity of η_{tc}. It also investigates the uncertainties due to temperature estimation errors and semiconductor parameter variations. Assume that all the parameters experience a variation of 5%, according to the article presented in [28], the temperature-related lifetime constants and the equivalent junction temperature swing can be modeled by the normal probability density function. Suppose that 10 000 samples are chosen to build up the distribution of η_{tc}. Fig. 11 shows the mean value μ of η_{tc} in the Monte Carlo analysis. It can be seen from Fig. 11 that the uncertainties make the values of η_{tc} vary. Nevertheless, the maximum η_{tc} with and without considering the uncertainties occur at the same $\Delta T_{j,\text{ref}}$. This indicates that the uncertainties would lead to the variation of η_{tc} but it has little impact on $\Delta T_{j,\text{ref}}$.

IV. Validation of the Proposed Strategy

The lifetime test is time consuming [30], and experimental tests over several years usually are not carried out in the laboratory. Nonetheless, computation of the consumed lifetime has been reported by previous studies [5], [22]. Thus, the tests are used to verify that the proposed method does not need to obtain the $\Delta T_{j,\text{MP}}$ in real time when $\Delta T_{j,\text{ref}}$ is determined. The performance of $\Delta T_{j,\text{ref}}$ is demonstrated by the case studies in different years and different locations. The Infineon FF1000R17IE4 IGBT module has voltage rating of 1700 V and current rating of 1000 A. Since the laboratory facilities cannot perform the tests with such high current and voltage, the IGBT module (2MBI75XAA170-50) with smaller power rating was adopted in the experiment.

A. Experimental Validation

A three-phase two-level inverter was constructed to perform the experimental validation. Fig. 12 depicts the experimental platform. The IGBT module was mounted on a forced air cooling heat sink with thermal grease. The junction temperature was measured by *IR* camera (Optris LTF-CF2) with $1\,\text{K/s}$ sample rate and $\pm 1\,^{\circ}\text{C}$ accuracy level. Since the silica gel would impede the temperature measurement, it was removed and the surface

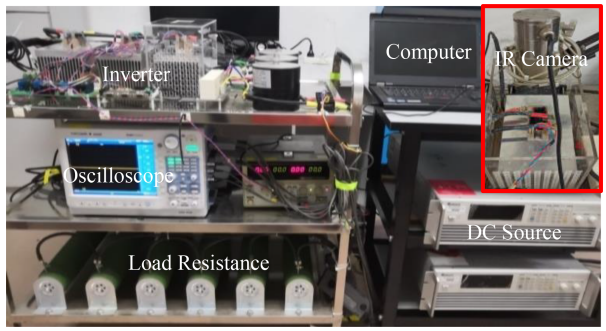

Fig. 12. Experimental platform.

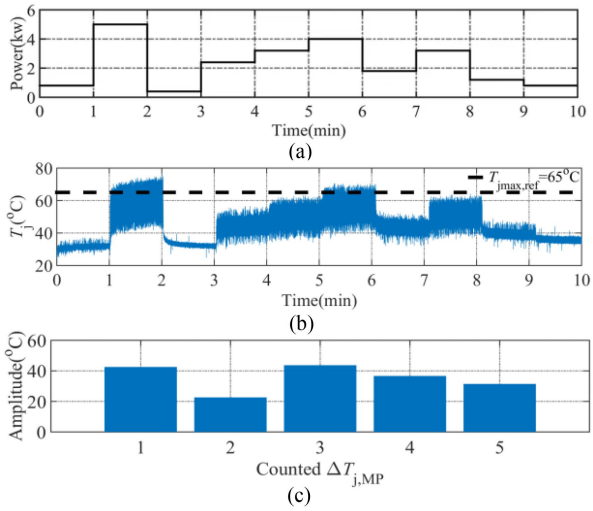

Fig. 13. Historical situation. (a) Power profile. (b) Junction temperature profile. (c) Counted $\Delta T_{j,\text{MP}}$ by rainflow algorithm.

of the chip was painted black to have a uniform and high emissivity. The emissivity of the black-painted surface is 0.97. It was obtained by heating the black-painted IGBT module to a fixed temperature on a temperature-controlled heating platform and calibrating the setting of *IR* camera to make the measured temperature consistent with the heated temperature. The dc-link voltage was set to 100 V because the open capsule module has a lower insulation voltage. Other parameters include the load resistance of 0.5 Ω, the switching frequency of 10 kHz, and T_a set to $25\,^{\circ}\text{C}$. The power of inverter was operated according to Fig. 13(a) to simulate the fluctuations of wind speed. This was considered as a historical situation in the test. The measured junction temperatures are shown in Fig. 13(b) and the counted $\Delta T_{j,\text{MP}}$ in Fig. 13(c).

It is observed from Fig. 13(c) that maximum $\Delta T_{j,\text{MP}}$ is about $43.5\,^{\circ}\text{C}$. Take $40\,^{\circ}\text{C}$ ripple as a target to illustrate that $\Delta T_{j,\text{MP}}$ can be regulated without the real-time acquisition. Based on the proposed strategy and (12), $T_{j\text{max,ref}}$ was set to $65\,^{\circ}\text{C}$. It means that the maximum T_j should not exceed $65\,^{\circ}\text{C}$. Otherwise, $\Delta T_{j,\text{MP}}$ would be greater than $40\,^{\circ}\text{C}$. The thermal control working range can be found with the help of Fig. 13(a) and (b). Thermal control is employed when the operating power exceeds 4 kW because the T_j is higher than $65\,^{\circ}\text{C}$ in these working conditions. Here,

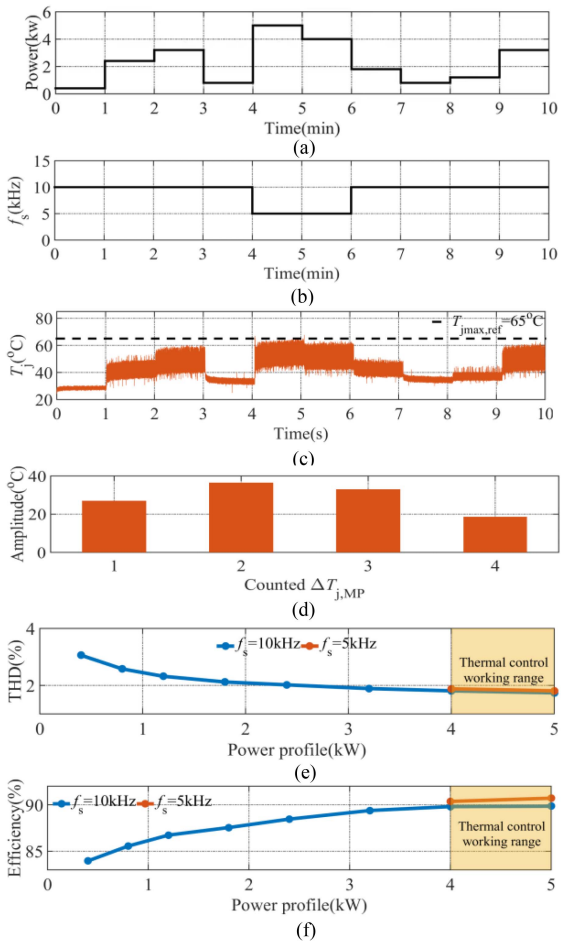

Fig. 14. Real-time situation. (a) Power profile. (b) Switching frequency. (c) T_j with thermal control. (d) Counted $\Delta T_{j,\mathrm{MP}}$. (e) THD. (f) Inverter efficiency.

T_j is controlled lower than the set limit of 65 °C by reducing f_s from 10 to 5 kHz.

Next, the operating power of inverter varies according to Fig. 14(a), which denotes the real-time situation. Fig. 14(b) shows the employed switching frequency and Fig. 14(c) shows the junction temperature profile with thermal control. The extracted $\Delta T_{j,\mathrm{MP}}$ values are listed in Fig. 14(d). The listed evidence shows that $\Delta T_{j,\mathrm{MP}}$ values ranged below 40 °C after thermal control. This result demonstrates that this strategy can regulate $\Delta T_{j,\mathrm{MP}}$ below $\Delta T_{j,\mathrm{ref}}$ without acquiring $\Delta T_{j,\mathrm{MP}}$ in real time, which reduces the complexity of thermal control. The effect on the inverter's electrical performance was also investigated. Results in Fig. 14(e) and (f) show that the inverter efficiency and THD increase in the working range of thermal control. This is mainly due to the reduction of switching frequency.

B. Case Validation

Since $\Delta T_{j,\mathrm{ref}}$ is designed based on the consumed lifetime with historical mission profile and the wind speeds are random and fluctuated, the question is: will the proposed strategy still work well for the future mission profile? To answer this question, case studies in different years are investigated, as shown in Table VI.

TABLE VI
RESULTS OF THE PROPOSED STRATEGY IN DIFFERENT YEARS

Location		Cavan		MalinHead	
Mission profile		Year 2017	Year 2018	Year 2017	Year 2018
CL_{F}(%)		1.23	2.33	70.32	68.07
CL_{M}(%)		14.87	18.70	66.49	64.53
$\Delta T_{\mathrm{j,ref}}$ (°C)	Type	$\Delta T_{\mathrm{j,MP}}$	$\Delta T_{\mathrm{j,MP}}$	$\Delta T_{\mathrm{j,FF}}$	$\Delta T_{\mathrm{j,FF}}$
	Amplitude	132	137	22	22
Maximum η_{tc} (%)		2.054	1.506	0.274	0.267
Actions of thermal control		$v_{\mathrm{th}} = 9.4m/s$ $T_{\mathrm{jmax,ref}} = 125.29$°C	$v_{\mathrm{th}} = 9.4m/s$ $T_{\mathrm{jmax,ref}} = 125.67$°C	$v_{\mathrm{th}} = 9.3m/s$	$v_{\mathrm{th}} = 9.3m/s$

TABLE VII
PERFORMANCE OF THE PROPOSED STRATEGY BASED ON DIFFERENT YEARS

Performance year	2018			
Location	Cavan		MalinHead	
Actions of thermal control	Based on 2017	Based on 2018	Based on 2017	Based on 2018
η_{tc}(%)	1.512	1.506	0.267	0.267
$n(\Delta T_{\mathrm{j}} > \Delta T_{\mathrm{j,ref}})$	0	0	0	0
CL'_{F}(%)	1.31	1.32	24.14	24.14
CL'_{M}(%)	11.17	11.20	22.85	22.85

It can be seen from Table VI that $\Delta T_{j,\mathrm{ref}}$ is obtained from $\Delta T_{j,\mathrm{MP}}$ in Cavan. Its value in 2017 is 132 °C and that in 2018 is 137 °C. They are not the same. This is mainly due to the variation of consumed lifetime. CL_M in 2017 is 14.87% and that in 2018 is 18.70%. Nonetheless, very similar actions of thermal control can be used to achieve the $\Delta T_{j,\mathrm{ref}}$ in different years.

To examine the performance of $\Delta T_{j,\mathrm{ref}}$, year 2017 data profile was used as the historical mission profile and year 2018 profile as the real-time situation. When the actions of thermal control based on 2017 were employed, almost the same impacts on year 2018 were obtained, as shown in Table VII. CL'_F and CL'_M denote the consumed lifetimes after thermal control under $\Delta T_{j,\mathrm{ref}}$. For example, the value of CL'_F was 1.31% when the actions determined based on 2017 data were performed in comparison to the value of 1.32% when the actions determined by the 2018 data were performed. In addition, when the actions of thermal control determined by 2017 profile were performed, the maximum η_{tc} was 1.512, which was very close to that obtained based on year 2018 profile. Thus, the $\Delta T_{j,\mathrm{ref}}$ selected based on the historical mission profile could offer guidance in the subsequent years. Besides, the $n(\Delta T_j > \Delta T_{j,\mathrm{ref}})$, which denotes the number of ΔT_j above $\Delta T_{j,\mathrm{ref}}$, becomes zero after thermal control. This confirms the proposition that "the proposed thermal control strategy does not need to obtain $\Delta T_{j,\mathrm{MP}}$ in real time." Similar results were also obtained in MalinHead.

V. PRACTICAL CONSIDERATIONS

A. Influence of the Error of Junction Temperature Estimation

The error between the estimated and measured junction temperatures affects the lifetime estimation but has little impact on the proposed strategy. To investigate the influence of error on the proposed strategy, we calculate the consumed lifetimes and

TABLE VIII
CONSUMED LIFETIMES AND THERMAL CONTROL EFFICIENCIES UNDER DIFFERENT ERRORS IN CAVAN

$\Delta T_{j,ref}$(°C)	Error = 0%			Error = 10%			Error = 20%			Error = 50%		
	CL(%)	CL'(%)	η_{tc}(%)	CL(%)	CL'(%)	η_{tc}(%)	CL(%)	CL'(%)	η_{tc}(%)	CL(%)	CL'(%)	η_{tc}(%)
134	14.87	10.59	2.029	21.41	15.25	2.918	29.88	21.28	4.074	70.22	50.01	9.576
133		10.26	2.006		14.78	2.886		20.62	4.029		48.46	9.469
132		**10.15**	**2.054**		**14.62**	**2.955**		**20.40**	**4.125**		**47.94**	**9.696**
131		9.81	2.007		14.14	2.887		19.72	4.030		46.35	9.471
130		9.71	2.048		13.99	2.946		19.52	4.113		45.86	9.666
129		9.37	1.985		13.50	2.856		18.84	3.987		44.27	9.371
128		9.28	2.020		13.36	2.906		18.65	4.057		43.82	9.534
127		8.92	1.933		12.85	2.781		17.93	3.882		42.13	9.123
126		8.83	1.961		12.72	2.822		17.75	3.939		41.71	9.258
125		8.52	1.889		12.28	2.718		17.13	3.794		40.26	8.917

The bold entities shows the best results is maximum η_{tc}.

TABLE IX
CONSUMED LIFETIMES AND THERMAL CONTROL EFFICIENCIES UNDER DIFFERENT ERRORS IN MALINHEAD

$\Delta T_{j,ref}$(°C)	Error = 0%			Error = 10%			Error = 20%			Error = 50%		
	CL(%)	CL'(%)	η_{tc}(%)	CL(%)	CL'(%)	η_{tc}(%)	CL(%)	CL'(%)	η_{tc}(%)	CL(%)	CL'(%)	η_{tc}(%)
27	70.32	61.96	0.068	116.02	102.07	0.113	183.89	161.58	0.181	608.12	532.68	0.613
26		52.93	0.133		87.04	0.221		137.55	0.354		451.61	1.196
25		44.41	0.186		72.88	0.310		114.96	0.495		375.68	1.670
24		37.09	0.225		60.74	0.375		95.62	0.599		311.01	2.015
23		30.50	0.255		49.83	0.424		78.29	0.676		253.30	2.272
22		**24.98**	**0.274**		**40.72**	**0.455**		**63.84**	**0.726**		**205.45**	**2.436**

The bold entities shows the best results is maximum η_{tc}.

thermal control efficiencies under different errors. The error is defined as

$$\text{Error} = \frac{T_j' - T_j}{T_j} \times 100\%. \tag{14}$$

In (14), T_j denotes the junction temperature without the error and T_j' that with error. Take the results in Cavan as an example. Tables VIII and IX present the values of CL, CL′, and η_{tc}, under different errors. CL′ denotes the consumed lifetime of power module after thermal control. It can be seen from Tables VIII and IX that the junction temperature error would lead to the variations of consumed lifetime and affects the thermal control efficiency η_{tc}. Moreover, it is observed that the maximum efficiency η_{tc} under different errors occur at the same $\Delta T_{j,ref}$, whether in MalinHead or Cavan. Since the proposed strategy selects $\Delta T_{j,ref}$ according to the maximum η_{tc}, the error has little impact on it.

B. Sensitivity of the Reference Junction Temperature Swing

Sensitivity of the reference junction temperature on the consumed lifetime can be analyzed using the mean junction temperature $T_{j,mean}$ by comparing the proposed approach with the normal approach. Table X presents the consumed lifetimes at different $\Delta T_{j,ref}$ by the proposed strategy and that at different $T_{j,mean}$ by the normal approach in MalinHead. Table XI presents the results in Cavan. It can be seen from Tables X and XI that the impact of $\Delta T_{j,ref}$ on the reliability of power module is more significant than that of $T_{j,mean}$. Take the results in MalinHead as example. The maximum $\Delta T_{j,ref}$ and $T_{j,mean}$ are 27.5 °C and 122.8 °C, respectively. The consumed lifetimes after thermal control CL′ are calculated from $\Delta T_{j,ref} = 27$ °C and $T_{j,mean} = 122$ °C. Table X presents that 1° difference between $\Delta T_{j,ref} = 27$ °C and $\Delta T_{j,ref} = 26$ °C can lead to 9.03% (= 61.96%−52.93%) difference in the consumed lifetime. In contrast, there is almost no difference about CL′ between $T_{j,mean} = 122$ °C and $T_{j,mean} = 112$ °C. This indicates that the

TABLE X
CONSUMED LIFETIMES UNDER DIFFERENT REFERENCES IN MALINHEAD

Proposed strategy		Normal approach	
$\Delta T_{j,ref}$ (°C)	CL' (%)	$T_{j,mean}$ (°C)	CL' (%)
27	61.96	122	70.32
26	52.93	112	70.31
25	44.41	102	70.16
24	37.09	92	68.69
23	30.50	82	63.81
22	24.98	72	57.65

TABLE XI
CONSUMED LIFETIMES UNDER DIFFERENT REFERENCES IN CAVAN

Proposed strategy		Normal approach	
$\Delta T_{j,ref}$(°C)	CL'(%)	$T_{j,mean}$(°C)	CL'(%)
134	10.59	112	14.87
133	10.26		
132	10.15	102	14.79
131	9.81		
130	9.71	92	14.32
129	9.37		
128	9.28	82	12.67
127	8.92		
126	8.83	72	10.44
125	8.52		

TABLE XII
COMPARISON OF DIFFERENT THERMAL CONTROL METHODS

Method	Are type and amplitude of $\Delta T_{\mathrm{j,ref}}$ required?	Need to acquire $\Delta T_{\mathrm{j,MP}}$ in real time?
Power loss regulation [7] [8] [9] [10] [11] [12] [13] [14] [15] [16]	No	Yes
Cooling system adjustment [17], [18]	No	Yes
Proposed strategy	Yes	No

consumed lifetime is more sensitive to the reference junction temperature $\Delta T_{j,\mathrm{ref}}$ than to the mean temperature $T_{j,\mathrm{mean}}$. Table XI offers a similar conclusion. For example, 1° difference from 134 to 133 °C in $\Delta T_{j,\mathrm{ref}}$ corresponds to 0.33% change in CL'. It takes 10° difference from 112 to 102 °C in $T_{j,\mathrm{mean}}$ for the change of 0.08% in CL'.

C. Comparisons With Other Methods

Table XII summarizes the features of different thermal management methods. It shows that the proposed strategy is able to provide the type and amplitude of $\Delta T_{j,\mathrm{ref}}$ but does not need to obtain the $\Delta T_{j,\mathrm{MP}}$ in real time. As a result, the benefit of thermal control is improved. For example, Table IV presents that the consumed lifetime reduced by each thermal control under $\Delta T_{j,\mathrm{ref}}$ is four times than that without considering $\Delta T_{j,\mathrm{ref}}$. In addition, this strategy can be employed without knowing the $\Delta T_{j,\mathrm{MP}}$ in the operation of wind turbine. Then, the wind speed forecasting can be removed and the thermal control becomes simple and efficient.

VI. CONCLUSION

In this article, a strategy to guide the selection of the reference junction temperature swing is presented. The proposed strategy provides a guideline for the selection of reference junction temperature swing, including the type and amplitude, which are chosen based on the distribution characteristics of consumed lifetime and the maximum thermal control efficiency, respectively. The benefit is the reduction of the consumed lifetime as much as possible at each application of the thermal control. More importantly, the proposed strategy does not need to obtain the junction temperature swing in real time when the reference of thermal control is determined. It is realized by considering the historical mission profile and sets the junction temperature at the valley as the minimum ambient temperature. This way, complexity of the thermal control is reduced and the thermal management is simple and efficient. The case studies and experimental results have been given to verify the performance of the proposed approach.

REFERENCES

[1] F. Blaabjerg, M. Liserre, and K. Ma, "Power electronics converters for wind turbine systems," *IEEE Trans. Ind. Appl.*, vol. 48, no. 2, pp. 708–719, Mar./Apr. 2012.

[2] H. Wang et al., "Transitioning to physics-of-failure as a reliability driver in power electronics," *IEEE J. Emerg. Sel. Topics Power Electron.*, vol. 2, no. 1, pp. 97–114, Mar. 2014.

[3] K. Fischer et al., "Reliability of power converters in wind turbines: Exploratory analysis of failure and operating data from a worldwide turbine fleet," *IEEE Trans. Power Electron.*, vol. 34, no. 7, pp. 6332–6344, Jul. 2019.

[4] L. R. GopiReddy, L. M. Tolbert, and B. Ozpineci, "Power cycle testing of power switches: A literature survey," *IEEE Trans. Power Electron.*, vol. 30, no. 5, pp. 2465–2473, May 2015.

[5] D. Weiss and H.-G. Eckel, "Fundamental frequency and mission profile wearout of IGBT in DFIG converters for windpower," in *Proc. 15th Eur. Conf. Power Electron. Appl.*, Lille, France, 2013, pp. 1–6.

[6] M. Held, P. Jacob, G. Nicoletti, P. Scacco, and M.-H. Poech, "Fast power cycling test of IGBT modules in traction application," in *Proc. 2nd Int. Conf. Power Electron. Drive Syst.*, 1997, pp. 425–430.

[7] D. Xiang, C. Wang, and Y. Liu, "Switching frequency dynamic control for DFIG wind turbine performance improvement around synchronous speed," *IEEE Trans. Power Electron.*, vol. 32, no. 9, pp. 7271–7283, Sep. 2017.

[8] J. Zhang, X. Du, C. Qian, R. Du, X. Hu, and H.-M. Tai, "Thermal management of IGBT module in the wind power converter based on the ROI," *IEEE Trans. Ind. Electron.*, vol. 69, no. 8, pp. 8513–8523, Aug. 2022.

[9] L. Wei, J. McGuire, and R. A. Lukaszewski, "Analysis of PWM frequency control to improve the lifetime of PWM inverter," *IEEE Trans. Ind. Appl.*, vol. 47, no. 2, pp. 922–929, Mar./Apr. 2011.

[10] Y. Ko, M. Andresen, G. Buticchi, and M. Liserre, "Discontinuous-modulation-based active thermal control of power electronic modules in wind farms," *IEEE Trans. Power Electron.*, vol. 34, no. 1, pp. 301–310, Jan. 2019.

[11] Y. Ko, J. Kuprat, S. Pugliese, and M. Liserre, "Modulation strategies for thermal stress control of CHB inverters," *IEEE Trans. Power Electron.*, vol. 37, no. 3, pp. 3515–3527, Mar. 2022.

[12] B. Wang, L. Zhou, Y. Zhang, K. Wang, X. Du, and P. Sun, "Active junction temperature control of IGBT based on adjusting the turn-off trajectory," *IEEE Trans. Power Electron.*, vol. 33, no. 7, pp. 5811–5823, Jul. 2018.

[13] D. A. Murdock, J. E. R. Torres, J. J. Connors, and R. D. Lorenz, "Active thermal control of power electronic modules," *IEEE Trans. Ind. Appl.*, vol. 42, no. 2, pp. 552–558, Mar./Apr. 2006.

[14] C. H. van der Broeck, L. A. Ruppert, R. D. Lorenz, and R. W. de Doncker, "Methodology for active thermal cycle reduction of power electronic modules," *IEEE Trans. Power Electron.*, vol. 34, no. 8, pp. 8213–8229, Aug. 2019.

[15] K. Ma, M. Liserre, and F. Blaabjerg, "Reactive power influence on the thermal cycling of multi-MW wind power inverter," *IEEE Trans. Ind. Appl.*, vol. 49, no. 2, pp. 922–930, Mar./Apr. 2013.

[16] Z. Li et al., "Active gate delay time control of Si/SiC hybrid switch for junction temperature balance over a wide power range," *IEEE Trans. Power Electron.*, vol. 35, no. 5, pp. 5354–5365, May 2020.

[17] X. Wang, A. Castellazzi, and P. Zanchetta, "Regulated cooling for reduced thermal cycling of power devices," in *Proc. 7th Int. Power Electron. Motion Control Conf.*, 2012, pp. 238–244.

[18] M. Onifade, A. Castellazzi, and P. Zanchetta, "Advances in the dynamic active cooling of power electronic modules," in *Proc. 6th IET Int. Conf. Power Electron., Mach. Drives*, 2012, pp. 1–5.

[19] Infineon Technologies, "AG: AN2019-05 PC and TC diagrams," Neubiberg, Germany, Feb. 2021.

[20] S. Ye, D. Zhou, X. Yao, and F. Blaabjerg, "Component-level reliability assessment of a direct-drive PMSG wind power converter considering two terms of thermal cycles and the parameter sensitivity analysis," *IEEE Trans. Power Electron.*, vol. 36, no. 9, pp. 10037–10050, Sep. 2021.

[21] M. Novak, V. Ferreira, M. Andresen, T. Dragicevic, and F. Blaabjerg, "FS-MPC based thermal stress balancing and reliability analysis for NPC converters," *IEEE Open J. Power Electron.*, vol. 2, pp. 124–137, 2021.

[22] S. D'Arco, T. M. Undeland, M. Bohlländer, and J. Lutz, "A simplified algorithm for predicting power cycling lifetime in direct drive wind power systems," in *Proc. 9th Int. Multi-Conf. Syst., Signals Devices*, 2012, pp. 1–6.

[23] M. Lei, L. Shiyan, J. Chuanwen, H. Liu, and Z. Yan, "A review on the forecasting of wind speed and generated power," *Renewable Sustain. Energy Rev.*, vol. 13, no. 4, pp. 915–920, May 2009.

[24] 2022. [Online]. Available: https://www.met.ie/climate/available-data/historical-data

[25] X. Du, Xiong Du, J. Zhang, and G. Li, "Numerical junction temperature calculation method for reliability evaluation of power semiconductors in power electronics converters," *J. Power Electron.*, vol. 21, pp. 184–194, 2021.

[26] H. Huang and P. A. Mawby, "A lifetime estimation technique for voltage source inverters," *IEEE Trans. Power Electron.*, vol. 28, no. 8, pp. 4113–4119, Aug. 2013.
[27] R. Bayerer, T. Herrmann, T. Licht, J. Lutz, and M. Feller, "Model for power cycling lifetime of IGBT modules—Various factors influencing lifetime," in *Proc. 5th Int. Conf. Integr. Power Electron. Syst.*, 2008, pp. 1–6.
[28] P. D. Reigosa, H. Wang, Y. Yang, and F. Blaabjerg, "Prediction of bond wire fatigue of IGBTs in a PV inverter under a long-term operation," *IEEE Trans. Power Electron.*, vol. 31, no. 10, pp. 7171–7182, Oct. 2016.
[29] A. Hanif, Y. Yu, D. DeVoto, and F. Khan, "A comprehensive review toward the state-of-the-art in failure and lifetime predictions of power electronic devices," *IEEE Trans. Power Electron.*, vol. 34, no. 5, pp. 4729–4746, May 2019.
[30] J. Falck, C. Felgemacher, A. Rojko, M. Liserre, and P. Zacharias, "Reliability of power electronic systems: An industry perspective," *IEEE Ind. Electron. Mag.*, vol. 12, no. 2, pp. 24–35, Jun. 2018.

Jun Zhang (Member, IEEE) received the B.S. degree from Anhui University, Hefei, China, in 2014, and the Ph.D. degree from Chongqing University, Chongqing, China, in 2019, both in electrical engineering.

He is currently a Lecturer with the College of Energy and Electrical Engineering, Hohai University, Nanjing, China. His research interests include the reliability of power electronics.

Dr. Zhang was a recipient of the Excellent Doctoral Dissertation of Chongqing Municipality in 2020.

Xiong Du (Member, IEEE) received the B.S., M.S., and Ph.D. degrees from Chongqing University, Chongqing, China, in 2000, 2002, and 2005, respectively, all in electrical engineering.

Since 2002, he has been with Chongqing University, where he is currently a Full Professor with the School of Electrical Engineering. He was a Visiting Scholar with Rensselaer Polytechnic Institute, Troy, NY, USA, from July 2007 to July 2008. His research interests include power electronics system reliability and stability.

Dr. Xu was a recipient of the National Excellent Doctoral Dissertation of China in 2008.

Cheng Qian received the B.S. degree in electrical engineering from Heilongjiang University, Harbin, China, in 2019. He is currently working toward the M.S. degree in electrical engineering with Chongqing University, Chongqing, China.

His research interests include reliability and thermal management of IGBT modules.

Yuyun Ye (Member, IEEE) received the B.E. degree in electrical engineering from Northeastern University, Shenyang, China, in 2015, and the M.E. degree in electronic and communication engineering from Sichuan University, Chengdu, China, in 2018. He is currently working toward the Ph.D. degree with the Department of Electrical and Computer Engineering, University of Tulsa, Tulsa, OK, USA.

His research interests include image processing and deep learning applications in power and energy.

Junjie Zhou received the B.S. degree in electrical engineering in 2020 from Chongqing University, Chongqing, China, where he is currently working toward the M.S. degree in electrical engineering.

His research interests include reliability and condition monitoring of IGBT modules.